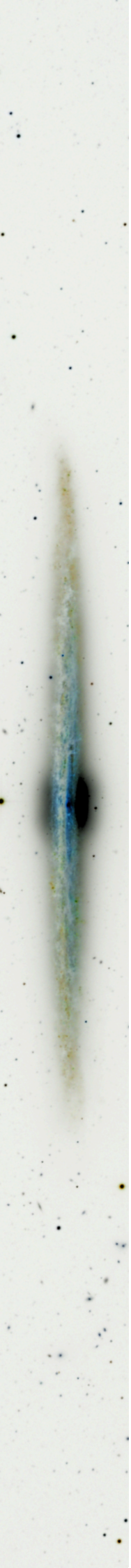

Universidad de La Laguna

Master's Degree in Astrophysics

Master's Thesis

Code for decomposing the discs of edge-on galaxies into their thin and thick components

Cecilia Arrizabalaga Díaz-Caneja

July 2024

supervised by
Dr. Sébastien Comerón

Acknowledgements

First of all, I would like to thank my parents María Luisa and Gotzon for their immeasurable and endless support, reminding me of my competence and encouraging me to continue. In addition, I would also like to thank Juanma, always ready to reassure and motivate me, Alicia, who has pushed me to work by transmitting her own anxiety to me, and my friends Nerea, Zuriñe and María, experts in distracting me with good plans and conversations.

Finally and necessarily, I would like to thank my supervisor, the teacher Dr. Sébastien Comerón, for guiding me and helping me in this work. Without his previous knowledge, experience, and quick corrections, it would have taken me ages to finish this project.

En primer lugar, quiero agradecer a mis padres María Luisa y Gotzon por su incontable e inagotable apoyo, recordándome mi competencia y animándome a seguir. Además, quiero también agradecer a Juanma, siempre dispuesto a tranquilizarme y alentarme, a Alicia, que me ha empujado a trabajar al contagiarme su propio agobio, y a mis amigas Nerea, Zuriñe y María, expertas en distraerme con buenos planes y conversaciones.

Final e ineludiblemente, quiero agradecer a mi supervisor, el docente Dr. Sébastien Comerón, por orientarme y ayudarme en este trabajo. Sin su conocimiento, previa experiencia, y rápidas correcciones, habría tardado siglos en terminar este proyecto.

Lehenik eta behin, eskerrak eman nahi dizkiet nire gurasoei, María Luisa eta Gotzoni, beren laguntza neurtezin eta agortezinagatik, nire gaitasuna gogoraraziz eta jarraitzera animatuz. Gainera, eskerrak eman nahi dizkiot Juanmari, beti lasaitzeko eta animatzeko prest, Aliziari, bere kezka transmitituz lan egitera bultzatu bainau, eta nire lagunei, Nerea, Zuriñe eta Mariari, plan eta elkarrizketa onekin arreta galarazten didaten adituak.

Azkenik, eta halabeharrez, eskerrak eman nahi dizkiot nire tutoreari, Sébastien Comerón doktoreari, lan honetan lagundu eta gidatzeagatik. Bere aurretiko ezagutza, esperientzia eta zuzenketa azkarrik gabe, urteak behar izango nituzke proiektu hau amaitzeko.

Front cover picture: L−RGB image of NGC 4565 taken by Ken Crawford.

Resumen

Las galaxias de disco, como la Vía Láctea, tienen un disco grueso y un disco delgado. El disco grueso tiene una mayor altura de escala que el disco delgado. El estudio de las poblaciones estelares del disco grueso de nuestra galaxia han demostrado que sus estrellas son más antiguas y menos metálicas que las del disco delgado. Según algunas hipótesis esta componente se formó en las primeras etapas turbulentas de la galaxia. El disco delgado contiene estrellas más jóvenes y ricas en metales.

Este trabajo presenta un nuevo código escrito en Python que extrae perfiles de brillo superficial de una imagen de galaxia de canto. Se modela el perfil de brillo superficial perpendicular al plano de la galaxia con un modelo que se obtiene resolviendo numéricamente las ecuaciones de equilibrio hidrostático para dos discos isotermos acoplados. De esta forma podemos conocer la contribución del disco delgado y del disco grueso a un determinado radio, así como sus alturas de escala. Nuestro principal objetivo es desarrollar un código Python que sea rápido, modular y fácil de usar para mejorar la investigación sobre galaxias de canto y poder en futuros estudios caracterizar la evolución de la estructura vertical de discos gruesos con el desplazamiento al rojo. La importancia de estos estudios radica en que su investigación puede aportar información sobre los mecanismos de formación de los discos.

Para este trabajo se seleccionaron las galaxias ESO 533-004 y NGC 4565, ambas galaxias del S^4G tomadas a 3,6 μm, debido a su claridad e idoneidad para un análisis comparativo detallado con los resultados de Comerón et al. (2018). El preprocesamiento de los datos observacionales incluyó rigurosos pasos para mejorar la calidad y precisión de los datos. Entre ellos se incluyó la sustracción del fondo de cielo y la interpolación sobre regiones enmascaradas para rellenar huecos en los datos. Para optimizar el análisis de los perfiles de brillo superficial, se seleccionaron estratégicamente intervalos axiales para captar las variaciones a lo largo del radio de la galaxia.

Para obtener los perfiles de brillo superficial se empleó un proceso iterativo que implicaba el desplazamiento de las imágenes para determinar el plano medio de la galaxia con una precisión de subpíxel. Se generaron perfiles sintéticos mediante la resolución de ecuaciones diferenciales, simulando los perfiles verticales de densidad de los discos grueso y delgado de las galaxias, transformados posteriormente en perfiles de brillo superficial. Estos modelos se escalaron cuidadosamente y se ajustaron a los datos observados.

Tras resolver las ecuaciones diferenciales para modelar los perfiles de brillo superficial, el siguiente paso crucial es la convolución. Este proceso integra el perfil de brillo superficial del modelo con la función de dispersión lineal (LSF), que modela los efectos del sistema de imagen óptico en los perfiles sintéticos. Este paso es esencial para poder comparar el perfil sintético con el observado.

Conseguir un ajuste preciso de las contribuciones de los discos delgados y gruesos requiere un enfoque iterativo. Este proceso comienza con un rango dinámico mínimo $\Delta\mu = 4{,}5\,\mathrm{mag\,arcsec^{-2}}$. Aumentando iterativamente en $0{,}5\,\mathrm{mag\,arcsec^{-2}}$, se controla el error cuadrático medio (RMSE) para garantizar la convergencia con un RMSE inferior a $0{,}1\,\mathrm{mag\,arcsec^{-2}}$, lo que indica un ajuste fiable. Los pasos clave de este proceso iterativo incluyen la normalización del perfil

observado, el cálculo de los perfiles de densidad sintéticos mediante las ecuaciones diferenciales y la convolución del modelo con la LSF.

En el proceso de verificación de la fiabilidad del modelo frente a estudios anteriores concluimos que los resultados son consistentes con los de Comerón et al. (2018), confirmando la robustez del modelo. Además vemos que NGC 4565 tiene un disco delgado más prominente que ESO 533-004, hecho que concuerda con la teoría 'downsizing' aplicada a discos. La teoría postula que las galaxias más masivas como NGC 4565 están más evolucionadas. En el supuesto de que los discos gruesos se formen primero y luego más lentamente los discos delgados, las galaxias masivas como NGC 4565 tendrían discos delgados más desarrollados. Además, los ratios de velocidades de dispersión sugieren trayectorias evolutivas o mecanismos de formación distintos para los discos grueso y delgado.

Las discrepancias entre nuestros resultados y los de Comerón et al. (2018) probablemente se deban a diferencias metodológicas como la exclusión del disco de gas en nuestro modelo, el tratamiento de los píxeles enmascarados mediante interpolación y el uso de un modelo LSF simplificado, entre otras. Las posibles futuras implementaciones al código podrían incluir la incorporación del disco de gas, el modelado del efecto del bulbo galáctico, el refinamiento del modelo LSF, y potencialmente la introducción de una Υ_T/Υ_t variable para mejorar la fidelidad del modelo, donde Υ_T/Υ_t es el ratio entre las relaciones masa-luz de los discos grueso y delgado que se utiliza para convertir perfiles de densidad en perfiles de brillo superficial.

Contents

Abstract

This study introduces a code that generates and fits vertical surface brightness profiles in edge-on galaxies with synthetic profiles created using thin and thick disc models derived from hydrostatic equilibrium equations for two coupled isothermal discs. Using advanced observational techniques and sophisticated modelling, the vertical structure of ESO 533-004 and NGC 4565, from the S^{4}G survey at 3.6 μm, is analysed. The methodology addresses scattered light effects with the Line Spread Function (LSF), a rigorous data preprocessing, and iterative fitting processes. The verification against previous studies confirms the model reliability, showing consistency in the results. We find that, relative to the mass of the galaxy, the thin disc is more massive in NGC 4565. Some disc formation models suggest that thick discs form first and then thin discs emerge at a slower rhythm. Our results support these models, as in the framework of a Universe with downsizing massive galaxies, like NGC 4565, are more evolved than lower-mass galaxies and therefore have time to fully grow a thin disc. Future implementations may include incorporating gas discs and refining the LSF model.

1 Introduction

The study of disc galaxies has significantly advanced our understanding of the evolution of the Universe. At high redshift, the Universe was uniform and homogeneous, a period characterized by the absence of complex structures. Over time, however, gravitational instabilities led to the formation of galaxies and the large-scale structure of the Universe. One of the challenges of modern astronomy is to understand the formation of galaxies from the early nearly homogeneous early Universe.

Up until about 30 years ago, observing galaxies at high redshift was extremely difficult due to technological limitations. Consequently, astrophysicists relied on the study of nearby galaxies to infer their formation processes, a method often referred to as Galactic Archaeology. This approach involved examining the properties and composition of local galaxies to reconstruct their evolution histories. Nowadays Galactic Archaeology can be complemented by the study of galaxies at high redshift thanks to the *Hubble Space Telescope (HST)* and the *James Webb Space Telescope (JWST)* imaging, as well as with advanced ground-based facilities.

Our current knowledge of disc galaxy formation has been influenced by a number of important discoveries. In 1979, it was brought to light that external galaxies possess both thin and thick discs (Burstein, 1979; Tsikoudi, 1979). This finding was later confirmed for the Milky Way by Gilmore & Reid (1983). In our galaxy the thick disc is older than the thin disc (Bensby et al., 2005) and more α-enhanced and metal-poor (Prochaska et al., 2000). Its scale height is around one kiloparsec, while that of the thin disc is about a few hundred parsecs.

These discoveries raised numerous questions about the formation mechanisms of these discs, prompting further research and debate in the scientific community. In their paper about galactic evolution, Kormendy & Kennicutt (2004) provided a chart that outlines various mechanisms involved in evolutionary processes that shape galaxies and that can be applied to thick discs. Fig. 1 shows a simplified version of the morphological box in Kormendy & Kennicutt (2004).

Researchers have proposed several

mechanisms to explain the formation of thick discs in galaxies, categorized broadly into internal and external processes, each operating on different timescales. The main four mechanisms, corresponding to the four quadrants in Fig. 1, are the following:

1. Fast Internal Evolution:

   At high redshift, galaxies contained significantly more gas than nowadays, as there had not been enough time to transform much gas into stars. Some theories suggest that the specific rate at which stars are formed is directly related to the surface density of gas present. Consequently, higher gas surface density results in more star formation, which results in more turbulence, resulting in the formation of a thicker disc where the stars form. When gas is depleted, the star forming rate decreases and the star formation continues in a thin disc. This mechanism is proposed in the work of Elmegreen & Elmegreen (2006), Bournaud et al. (2009) and Comerón et al. (2014).

2. Slow Internal Evolution:

   According to Villumsen (1983) an initially thin disc thickens over time due to scatter caused by spiral arms, giant molecular clouds and interactions among its stars, along with other things. As new stars form, they create a thin disc. Schönrich & Binney (2009a,b) and Roškar et al. (2013) proposed refinements of this process in their studies.

3. Fast External Interactions:

   In this scenario, during the early stages of galaxy formation, gas-rich fragments come together and merge. These mergers are often chaotic and result in the formation of a thick disc due to the turbulent and dynamic interactions of the merging fragments. After this process the remaining and nearly accreted gas forms a new thin disc. Brook et al. (2004) and Martig et al. (2014a,b) discuss this mechanism in their work.

4. Slow External Interactions:

   In the works of Abadi et al. (2003a,b) and Qu et al. (2011a,b) it is suggested that a thin disc can thicken through the accretion of satellite galaxies and the perturbations caused by these interactions.

In reality, the formation of thick discs likely involves a combination of these four mechanisms. The dominant mechanism may vary depending on specific galactic conditions such as the mass or the environment (Comerón et al., 2012).

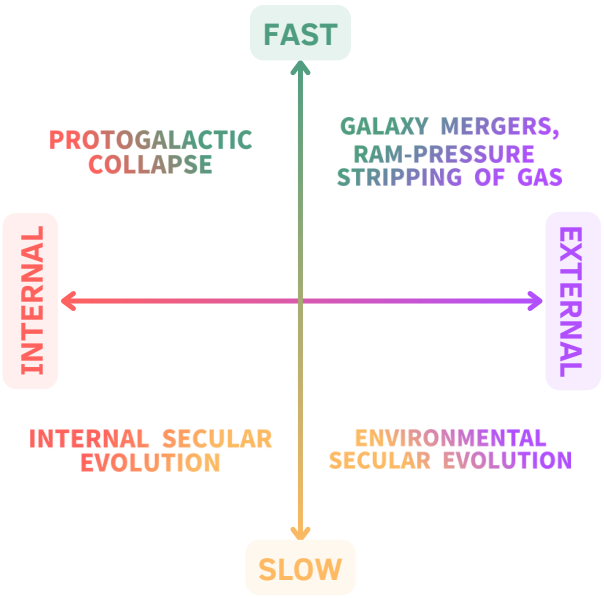

Figure 1: Diagram of galactic evolution processes based on the morphological box of Kormendy & Kennicutt (2004). The processes are ordered in the different axes according to their timescales and nature: from fast (top) to slow (bottom), and from internal (left) to external (right).

Recent studies have provided further insights into disc galaxy formation through advanced observational techniques and detailed

analysis, being one them the Integral Field Unit (IFU) spectroscopy, often called 3D spectroscopy, which aims to obtain spectra at all the points in a 2D image at the same time. Using this technique the Pinna et al. (2019a,b) studies focused on three S0-type galaxies in the Fornax cluster. The results indicated that the old thick disc has a chemical composition indicative of a galaxy formed rapidly through mechanisms 1 and an accretion of stars at a level of $\sim$ 20 % of the mass of the thick disc, as suggested by mechanism 4 mentioned above. The thin disc, more extended horizontally than the thick disc, exhibits flares in the outer regions due to lower density and increased susceptibility to perturbations. Geometrically, these flares might appear as a thick disc, but stellar population studies confirm them as part of the chemical thin disc.

Another interesting work using this observing technique is the one led by Sébastien Comerón (Comerón et al., 2016), where they studied another S0 galaxy in a cluster. Their study revealed an old, metal-poor thick disc alongside an old, metal-rich thin disc. This finding suggests that massive galaxies can lose gas before completing the formation of their thin discs.

Comerón et al. (2015) suggest that mechanisms 1 and 2 could be the favoured mechanisms for the formation of thick discs, by comparing their properties across multiple galaxies. These processes are capable of explaining the observed characteristics of thick discs, such as their old stellar populations, low-metallicities and lack of retrograde material. Comerón et al. (2019) studied the latter characteristic by observing eight galaxies with the integral field unit MUSE instrument at the VLT. In their work they notice the absence of evidence for a significant fraction of retrograde material in eight late-type field galaxies. These results suggest that the thick-disc origin is either an internal origin or a situation in which an existing thin disc is dynamically heated by interactions, ruling out accretion as the primary thick-disc formation mechanism for most galaxies.

Additional photometric studies like Comerón et al. (2011a,b, 2012, 2018) analysed the ratio of thick to thin disc mass ($\mathcal{M}_{\rm Thick}/\mathcal{M}_{\rm thin}$) as a function of the circular velocity of the galaxy ($v_{\rm c}$), that is proportional to the total mass $\mathcal{M}_{\rm total}$, observing a declining trend. This shows that less massive galaxies tend to have relatively more massive thick discs, while massive galaxies have less massive thick discs. Low-mass galaxies may not have developed a thin disc yet due to downsizing. If thick discs formed first and the thin discs followed at a slower rate, massive galaxies are expected to have more developed thin discs. This is because their stars formed at an earlier and quicker pace compared to lower mass galaxies and therefore are more evolved than the latter (Comerón et al., 2014; Comerón, 2021).

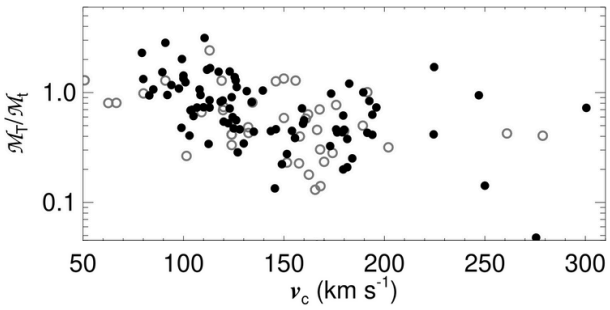

Figure 2: Ratio of the thick and the thin disc masses $\mathcal{M}_{\rm Thick}/\mathcal{M}_{\rm thin}$ as a function of $v_{\rm c}$. Figure obtained from Comerón et al. (2018).

The arrival of the *James Webb Space Telescope (JWST)* has transformed the field of astrophysics, especially in the research of distant galaxies at high redshifts. Therefore, it is crucial to create effective and easy-to-use computational tools in order to fully make use of the capabilities of the *JWST*. In the future

we intend to use archival data of deep fields and find hundreds to thousands of edge-on galaxies to study the evolution of thin and thick discs with redshift, for which we need to produce thin and thick disc decompositions, so a fast code is utmost essential. The code employed in Comerón's works (Comerón et al., 2011a,b, 2012, 2018), which was written in Interactive Data Language (IDL), presented significant limitations. It was in fact running very slow and was very arduous to modify due to its lack of modularity. This work presents a new code written in Python that extracts surface brightness profiles from an edge-on galaxy image and fits a synthetic profile derived from the models of the thin and thick discs obtained solving numerically the equations of hydrostatic equilibrium for two coupled isothermal discs. Our main goal is to develop a Python code that is fast, modular, and user-friendly to continue researching on edge-on galaxies and the vertical structure evolution of thick discs with redshift. The rationale behind its importance is that measuring thick disc masses as a function of redshift, host type or mass, and environment can give insight into disc formation mechanisms.

2 Methodology

2.1 General information

2.1.1 Used data

For this work we used images of two different galaxies: ESO 533-004 and NGC 4565, both from the S^{4}G - the *Spitzer* Survey of Stellar Structure in Galaxies at 3.6 μm (Sheth et al., 2010; Muñoz-Mateos et al., 2015). These images were taken with the Infrared Array Camera (IRAC) and have a 0.″75 pixel size. Each of these galaxies was observed for 240 s, resulting in a limiting magnitude of around $\mu_{3.6\mu m} = 26.5(\mathrm{AB})\ \mathrm{mag\,arcsec^{-2}}$.

In order to obtain the surface brightness profiles of the galaxies and study their vertical structure edge-on galaxies are needed. The reason for the selection of these two galaxies, ESO 533-004 and NGC 4565, is to conduct a comparison with the previous work of Comerón et al. (2018), where they reviewed the vertical structure of 141 edge-on disc galaxies (including ESO 533-004 and NGC 4565) by analysing 3.6μm images with an extended point spread function model that accounts for extended wings. These two specific cases were chosen due to their relatively clean appearance and well-defined structure, making them ideal candidates for testing the new software.

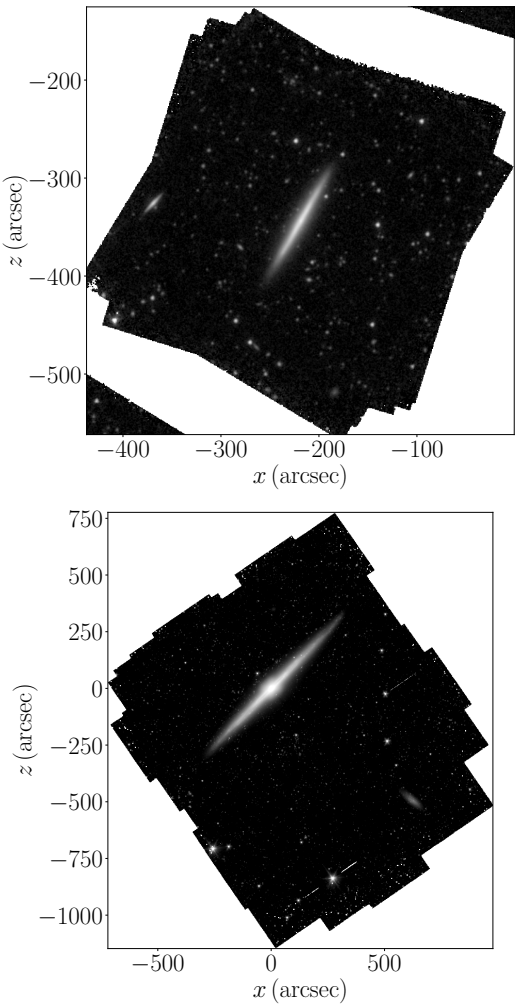

Figure 3: From top to bottom, the S^{4}G images of ESO 533-004 and NGC 4565 at 3.6 μm, respectively.

```
FILE | MASK | XC (pix) | YC (pix) | PA (deg) | SKY | PIX_SCALE (arcsec) | R_OPT (arcsec) | ZP |
BIN CENTRAL POSITION (IN FRACTION OF RADIUS) | BIN TOTAL WIDTH (IN FRACTION OF RADIUS) | LSF FILE
NAME

ESO533-004.phot.1.fits ESO533-004.mask.fits 582.90 749.07 150.5 0.060501 0.75 54.6 21.09669
-0.65,-0.35,0.35,0.65 0.30 PSF_mockgal.txt
NGC4565.phot.1.fits NGC4565.mask.fits 960.19 1529.92 135.1 0.032761 0.75 497.9 21.09669
-0.65,-0.35,0.35,0.65 0.30 PSF_mockgal.txt
```

Figure 4: Snapshot of the data file format for the correct functioning of the code.

Along with the pictures, a file with some characteristics of the images is needed as an input for the code. Fig. 4 shows an example of a possible input file. The file must contain the following information:

- Image file name.
- Mask file name (see Sect. 2.2.1).
- Centre x-axis pixel value of the galaxy.
- Centre y-axis pixel value of the galaxy.
- Position angle of the galaxy in degrees.
- Sky background value.
- Pixel scale value of the image in arcseconds.
- Optical radius of the galaxy in arcseconds.
- Zero Point value.
- Central positions of the bins separated by a comma without a space, in units of the optical radius (see Sect 2.2.2).
- Total width of the bins in units of the optical radius.
- Line Spread Function file name (see Sect. 2.1.2 for a definition).

In order to obtain the surface brightness profiles of these galaxies, a pre-processing of the images must be done, as explained in Sect. 2.2.1.

2.1.2 The line spread function

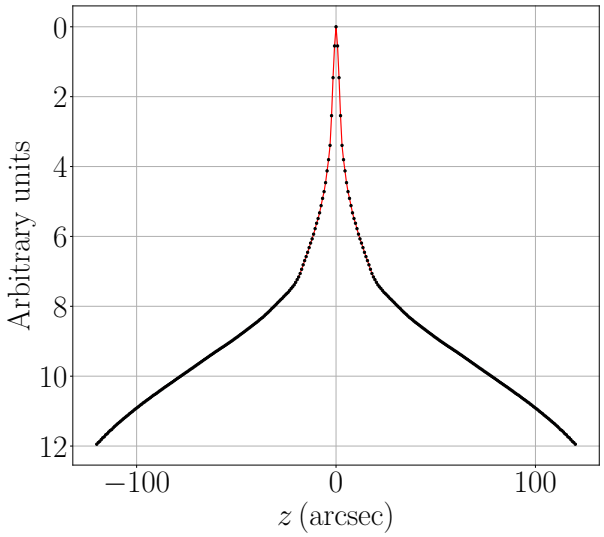

Figure 5: Line Spread Function scaled to the size of the S^{4}G pixel, 0.″75. The extended PSF has a pixel size of 0.″24, the same as the PSF.

Comparing observed data with synthetic data requires convolving the latter with a Point Spread Function (PSF), which characterizes how a focused optical imaging system responds to a point source. One significant challenge in this field is the effect of scattered light, which can distort the light distribution of galaxies. De Jong (2008) and Sandin (2015) stated that when convolving the image of a very thin edge-on galaxy with a Point Spread Function (PSF), the broad wings of the PSF can introduce artefacts that create a spurious thick disc or a stellar halo. In a very thin edge-on galaxy, most of the light is concentrated in a thin region along the plane

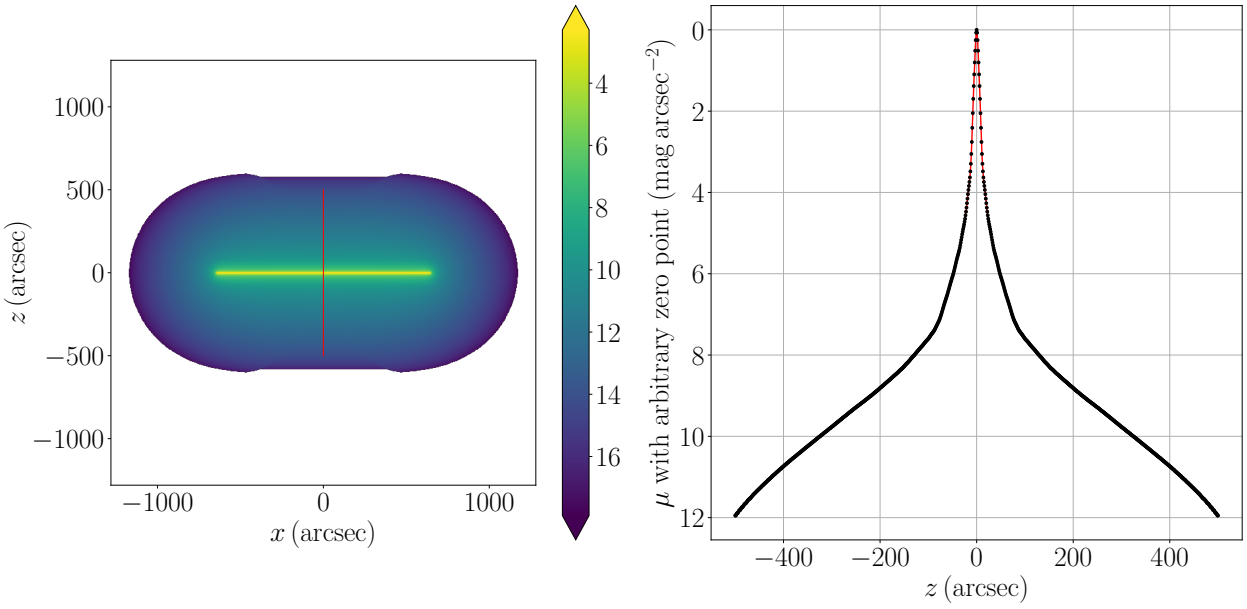

Figure 6: On the left, the infinitesimally thin mock galaxy convolved with the S^{4}G PSF. On the right, the LSF before rescaling to the pixel scale of the images. The vertical red line in the image on the left represents the cut to obtain the LSF.

of the disc. When convolved with a PSF, the light from this thin disc is spread out by the PSF's wings, creating an artificial thickening in the image.

This erroneous analysis can result in inaccurate conclusions about the structure and characteristics of the galaxy and makes us overestimate the thick disc contribution. As a result, proper modelling of the effects of the PSF is required to determine the true structure of the galaxy.

In this work we make use of a Line Spread Function (LSF) introduced by Elmegreen et al. (2017) and Comerón et al. (2018), a concept derived from the Point Spread Function (PSF) that defines how light from an infinitesimally thin distribution of light with an infinite extension, rather than a point source, spreads out in an image. This is a valid approach for objects such as edge-on galaxies, where one dimension (length) is much larger that the other (height).

The procedure to obtain the LSF is as follows: first, an infinitesimally thin mock galaxy is generated. For this project its dimensions must be at least the same as the provided by the Point Spread Function image of the telescope, which are 1281×1281 pixels. Then, this synthetic galaxy is convolved with the PSF. From this convolved image a vertical cut is done in order to obtain a surface brightness profile. The last step is to rescale this brightness profile to the pixel scale of the detector: $0\farcs75$. The used PSF is the symmetrised version of the S^{4}G PSF of the warm mission model at 3.6μm, from Hora et al. (2012).

2.2 Preprocessing of images

The S^{4}G provides science-ready images. However, for our study further data processing must be made. With the purpose of acquiring vertical profiles from these images, we must subtract the sky background value (estimated in Comerón et al., 2018), interpolate over the masks, and rotate and cut

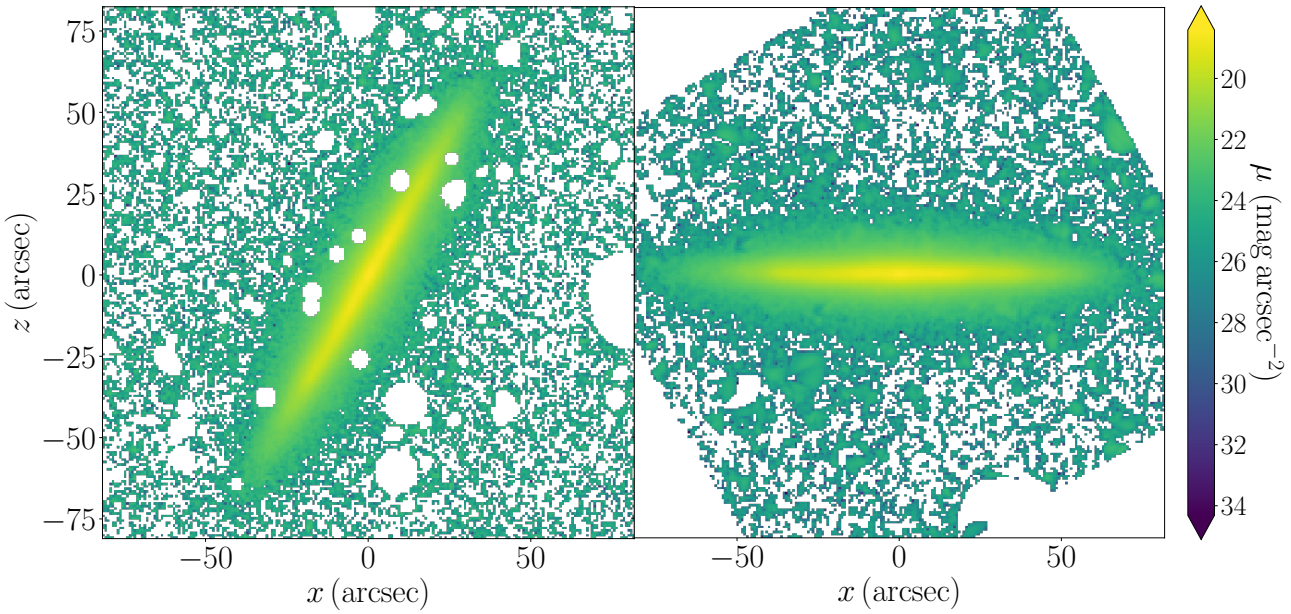

Figure 7: On the left, ESO 533-004 cropped and with the white regions indicating the mask.

the images so that the galaxy is centred and horizontal. The masks used in this work are the masks provided by the Pipeline 2 of the S^{4}G after being manually refined in Comerón et al. (2018).

2.2.1 Cutting the image and interpolating over the mask

The second of the four pipelines of the S^{4}G had the objective of generating masks for point sources in the field and nearby galaxies (Sheth et al., 2010; Muñoz-Mateos et al., 2015). These masks block bright objects like nearby stars on background galaxies so as to minimize their light contamination and improve the reliability of our results.

After the subtraction of the sky, the images were cut and centred in the galaxy. The dimensions of the cut are 3 times the optical radius of the galaxy. For this step it is important to make sure the galaxy fits well in the image. The target of the code in this step is to add rows and columns of zeros if they are needed, and then cut the image to the set dimensions.

Lastly the masked regions are filled with values interpolated using the `interpolate.CloughTocher2DInterpolator` sub-package of `scipy` in the code. Fig. 7 shows ESO 533-004 before and after these steps.

2.2.2 Selection of bins

To ensure a good signal-to-noise ratio when obtaining surface brightness profiles, we averaged the surface brightness over the width of axial bins. The bins containing these columns are represented in Fig. 8.

The parameters of the bins are their central position and their width. These numbers must be specified in the data file containing the information mentioned in Section 2.1.1. With the aim of comparing our results with the ones obtained by Comerón et al. (2018), the selected bins are $0.30 \times R_{\rm opt}$ wide, centred at positions $(-0.65, -0.35, 0.35, 0.65) \times R_{\rm opt}$, $R_{\rm opt}$ being the optical radius of the galaxy. This bin choice is intended to roughly display radial variations while steering clear of the bulge region where the thin plus thick

decomposition is no longer valid.

The position of each bin can be modified independently, while the width must be the same for all bins.

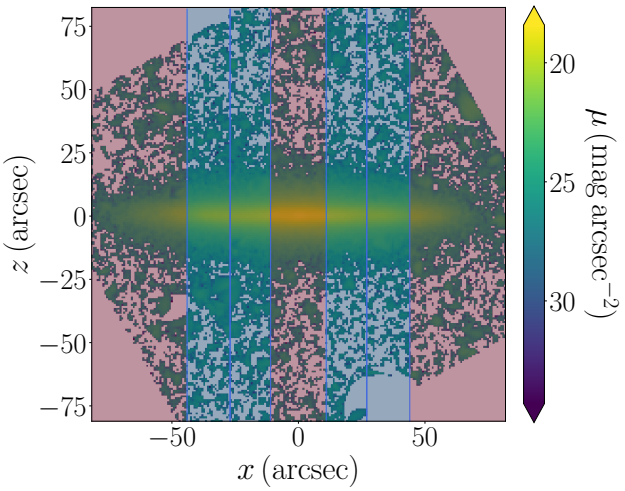

Figure 8: Image of ESO 533-004. The selected bins are represented in blue (see Sect. 2.2.2).

2.3 Obtaining the observed surface brightness profiles

The next step is to obtain the symmetrized surface brightness profiles of each galaxy, which requires first finding the mid-plane of the galaxy. Since we plan to use this software in the future for angularly small galaxies at high redshift observed with the *JWST*, achieving sub-pixel precision is essential. This can be accomplished by shifting the galaxy image up and down by fractions of a pixel. The number of shifts is an adjustable parameter in the code.

The obtention of the surface brightness profiles is done following an iterative process: in each iteration the image is shifted and the rows in the bins are averaged, obtaining the surface brightness profile along the whole height axis z. Then, the brightest value is found, and the profile is split in two. With these two half-profiles the RMSE (Root Mean Squared Error) is calculated in flux. For the obtention of the profile we only take into account data in a dynamical range of $\Delta\mu = 3\,\mathrm{mag\,arcsec^{-2}}$ to exclude the lowest surface brightness values, which are more prone to errors or external perturbations.

This process is repeated until all the shifts are done. When the loop finishes, the code finds the image shift with the smallest differences between the two halves: for this displacement, the symmetric values of the half-profiles are averaged obtaining the mean surface brightness profile.

2.4 Creating the synthetic surface brightness profiles

2.4.1 Differential equations

The synthetic profiles that we use to fit the observations are derived from the resolution of two coupled differential equations, the equations of hydrostatic equilibrium for two coupled isothermal discs. When solved numerically, these equations give the vertical density profiles of two gravitationally coupled isothermal discs, each with a different velocity dispersion σ:

$$\frac{d^2\rho_\mathrm{t}}{dz^2} = \frac{\rho_\mathrm{t}}{\sigma_\mathrm{t}^2}\left[-4\pi G\left(\rho_\mathrm{t}+\rho_\mathrm{T}\right)\right] + \frac{1}{\rho_\mathrm{t}}\left(\frac{d\rho_\mathrm{t}}{dz}\right)^2, \quad (1)$$

and

$$\frac{d^2\rho_\mathrm{T}}{dz^2} = \frac{\rho_\mathrm{T}}{\sigma_\mathrm{T}^2}\left[-4\pi G\left(\rho_\mathrm{t}+\rho_\mathrm{T}\right)\right] + \frac{1}{\rho_\mathrm{T}}\left(\frac{d\rho_\mathrm{T}}{dz}\right)^2, \quad (2)$$

where the subindexes t and T stand for the thin and thick discs, respectively. These equations were used in Comerón et al. (2011a,b, 2018) by applying Narayan & Jog (2002)'s formalism.

In these equations there are four free parameters: the central densities of the thin and thick discs (ρ_t and ρ_T) and their dispersion velocities (σ_t and σ_T). We can simplify these to two by implementing a couple of subtleties that are simple to program

(see Section 2.4.2).

It should be noted that the resolution of these equations gives the densities of the thin and thick discs along the vertical axis z. However, what the code fits are surface brightness profiles. To transform these densities into surface brightness profiles, the thin and thick disc solutions must be multiplied by $\Upsilon_{\rm t}$ and $\Upsilon_{\rm T}$ respectively. However, because of the surface brightness normalisation applied later in Sect. 2.4.2, we only need to introduce the ratio of the mass-to-light ratios of the thick and thin discs at 3.6μm, $(\Upsilon_{\rm T}/\Upsilon_{\rm t})_{3.6\mu{\rm m}}$.

In this work we have used a $(\Upsilon_{\rm T}/\Upsilon_{\rm t})_{3.6\mu{\rm m}}$ value of 1.2, the same as the one used in Comerón et al. (2018). It was calculated with the individual mass-to-light ratios of the thin and thick discs derived from the star formation history (SFH) model of the Milky Way in Nykytyuk & Mishenina (2006). Their model postulates a short initial star formation burst followed by an exponentially decaying star formation rate under the assumptions that the galactic disc can be divided into two distinct zones, the thin disc and the thick disc, and that each of these structures is presumed to have unique chemical characteristics and different evolutionary timescales.

2.4.2 Boundary conditions, normalisations and parameters

To solve these equations four boundary conditions are needed. Two of them imply that the maximum value of the surface brightness is in the mid-plane of the galaxy:

$$\begin{cases} \left.\dfrac{d\rho_{\rm t}}{dz}\right|_{z=0} = 0 \\ \\ \left.\dfrac{d\rho_{\rm T}}{dz}\right|_{z=0} = 0 \end{cases} \tag{3}$$

The other two would be the mid-plane density values of both discs:

$$\begin{cases} \rho_{\rm t}|_{z=0} \\ \\ \rho_{\rm T}|_{z=0} \end{cases} \tag{4}$$

The ratio of latter is a parameter to be fitted, as we will see next.

In order to minimize the computational complexity and memory requirements, it would be interesting to reduce the number of free parameters to be fitted. One way of doing this is normalising the profiles in surface brightness. Normalising the surface brightness profile to its mid-plane value sets a constraint that the sum of the mid-plane densities, weighted by their mass-to-light ratios, must be equal to a constant. By doing this, the mid-plane densities are no longer independent parameters and their ratio can be fitted instead, transforming from two free parameters into one.

Another way of decreasing the number of free parameters is scaling the height axis z. The profile is scaled so that at a certain height $z_{\rm c}$ the surface brightness is equal to that at the mid-plane multiplied by a factor f. Therefore, $z_{\rm c}$ is the height where the surface brightness profile of the observed data meets the synthetic profile at a surface brightness equal to f times the mid-plane value. This normalisation has the effect of removing the vertical scale, which results in reducing the two vertical velocity dispersion parameters into the ratio $\sigma_{\rm T}/\sigma_{\rm t}$.

As a result of these simplifications, the four free parameters have become two:

$$\begin{cases} \dfrac{\rho_{\rm T}|_{z=0}}{\rho_{\rm t}|_{z=0}} \\ \\ \dfrac{\sigma_{\rm T}}{\sigma_{\rm t}} \end{cases} \tag{5}$$

Unlike the approach of Comerón et al. (2018), where they used four set values of $f = 0.1, 0.2, 0.3, 0.4$, we introduce the factor f as a third free parameter to the routine doing the fit, with the purpose of computing the best fit.

2.4.3 Performing the convolution

Based on the solution of the differential equations shown in Eqs. 1 and 2, a model surface brightness profile is calculated. This model must be convolved with the LSF so that it can be compared with the observed one. This is done with the `scipy.signal.convolve()` routine of Python, using the Line Spread Function shown in Fig. 5.

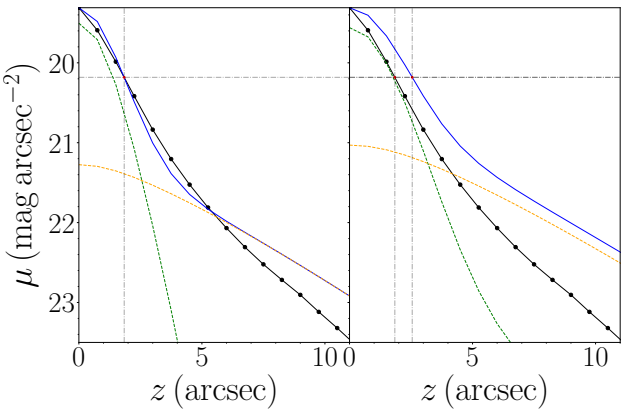

Figure 9: Comparison between the model before and after the convolution for the first iteration. The blue, green and yellow lines are the model of the total surface brightness and the thin and thick disc contribution models, respectively. The vertical and horizontal grey lines show the point where the model and the data should meet at flux μ_c (the central surface brightness multiplied by the factor f and then converted to magnitudes), in z_c which corresponds to a surface brightness $\mu_c = 20.18\,\mathrm{mag\,arcsec^{-2}}$. *On the left:* The models in the first iteration of the loop before the convolution process. The model and the observed data meet in z_c. *On the right:* The models in the first iteration of the loop after the convolution process and the flux renormalisation. The model and the observed data no longer meet in z_c. The convolved model now reaches a flux μ_c at a height $z'_c > z_c$.

Now, in the above subsection we mentioned that the vertical axis should be scaled to simplify the process of the resolution of the differential equations. For that, a scale must be obtained to rescale the synthetic vertical axis so that both z_c values (observed and synthetic) match at the height were the normalised flux is equal to f.

A technical problem that is encountered when the synthetic profile is convolved is that the height at which the observed and synthetic profiles cross has a flux f becomes $z'_c > z_c$, and the observed and synthetic profiles no longer cross at height z_c, as shown in Fig. 9. After convolution, the synthetic profile must be normalised in flux, z'_c must be calculated, and the vertical axis z must be rescaled multiplying it by a scale z_c/z'_c. This whole process is repeated until convergence. This convergence happens when criterion $z_c/z'_c > 0.9999$ is fulfilled. Further scrutiny has revealed that the iterations needed for the convergence of the z_c values depend on the galaxy: for ESO 533-004 the code needed 9 iterations, whereas for NGC 4565 it needed 3. This is expected: ESO 533-004 is a smaller galaxy and the PSF has a much larger effect, therefore it is harder to correct its effects. The number of needed iterations might also depend on the bin under study.

2.5 Obtention of the best fit

Achieving a detailed decomposition of the thin and thick discs requires a large dynamic range, because the thick disc usually manifests itself as a break in the slope of the surface brightness profile at large heights due to the predominance of the thin disc in the vicinity of the galactic mid-plane. According to Comerón et al. (2011a), a minimum dynamic range of $\Delta\mu = 4.5\,\mathrm{mag\,arcsec^{-2}}$ is considered necessary for achieving a reliable fit, so that is the initial dynamical range that the code uses.

The obtention of the fit is an iterative process: in each iteration the dynamic range value $\Delta\mu$ is increased by $0.5\,\mathrm{mag\,arcsec^{-2}}$, and at the end the RMSE is calculated. The following process is repeated as long as the RMSE does not exceed the value of $0.1\,\mathrm{mag\,arcsec^{-2}}$:

1. The observed surface brightness profile is normalised in flux.
2. With the initial values of $(\rho_\mathrm{T}|_{z=0})/(\rho_\mathrm{t}|_{z=0})$ and $\sigma_\mathrm{T}/\sigma_\mathrm{t}$ the synthetic density profiles of the thin and thick discs are calculated through equations 1 and 2.
3. The synthetic density profile of the thin disc is multiplied by $\Upsilon_\mathrm{T}/\Upsilon_\mathrm{t}$ to transform density profiles into surface brightness profiles. With the initial value of f, the z_c of the observed profile is obtained.
4. The iterative process to reach the convergence of the z_c values starts. We create a model from the sum of the contributions of the thin and thick discs.
5. This model is convolved with the Line Spread Function, it's normalised in flux and the z'_c value is obtained for the synthetic fit. Because of the convolution, $z'_\mathrm{c} > z_\mathrm{c}$.
6. A scale is calculated with the ratio of the observed z_c and synthetic z'_c. This scale is used to rescale the z axis for the synthetic profile.
7. Steps 4 through 6 are repeated until the scale tends to $z_\mathrm{c}/z'_\mathrm{c} \to 1$.
8. When the scale is $z_\mathrm{c}/z'_\mathrm{c} > 0.9999$, the RMSE between the fit in magnitudes and the observed profile is calculated.
9. If the RMSE $< 0.1\,\mathrm{mag\,arcsec^{-2}}$, the dynamic range $\Delta\mu$ is increased by $0.5\,\mathrm{mag\,arcsec^{-2}}$ and the coefficients of the fit ($(\rho_\mathrm{T}|_{z=0})/(\rho_\mathrm{t}|_{z=0})$, $\sigma_\mathrm{T}/\sigma_\mathrm{t}$ and f) become the initial values for the next iteration.
10. Steps 1 through 9 are repeated until the RMSE value exceeds $0.1\,\mathrm{mag\,arcsec^{-2}}$.

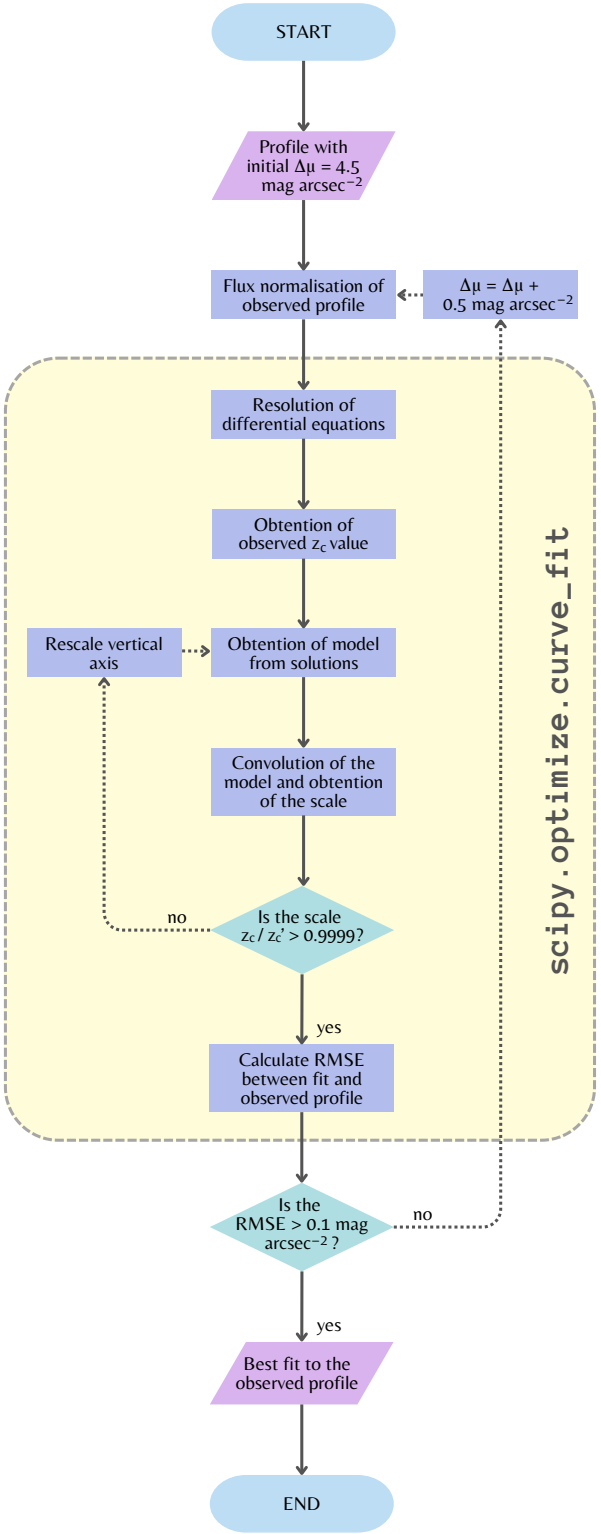

Figure 10: Flow diagram summarizing the fitting process described in Section 2.5.

Height_z_in_arcsec	Observed_profile_in_mag	Fit_profile_in_mag	Fit_of_thin_disc_in_mag	Fit_of_thick_disc_in_mag
0.0	19.968541000721597	19.968541000721597	20.14527238938524	22.026734886286707
0.75	20.068910154090368	20.0410567959565	20.2271532302593	22.047741960846093
1.5	20.32353386556776	20.2474632006649	20.463148525166304	22.10828048207751
2.25	20.657315038004686	20.55797419719754	20.82771624278196	22.20199354036395
...	...	...	...	...

(a) Snapshot of the file of the first bin of ESO 533-004: 'ESO533-004_bin_1.csv'.

Bin_number	Bin_position	Bin_width	Fit_parameter_1	Fit_parameter_2
1	-0.65	0.3	0.17877515278251552	2.1407314431534736
2	-0.35	0.3	0.21202243234196105	2.138507328913943
3	0.35	0.3	0.3516146184493814	2.5043958384107188
4	0.65	0.3	0.3425347545302737	2.341558745421874

Fit_parameter_3	Mass_to_light_ratio	Dynamic_range	RMSE_of_fit	Thick_thin_ratio
0.08656941354249498	1.2	5.0	0.05254119107941244	0.4913386718793843
0.06313936799352178	1.2	6.0	0.038824325447590104	0.5775671146513243
0.13725070491516514	1.2	7.0	0.08865896647599344	1.1513406770699932
0.18072267530807673	1.2	6.0	0.07902987602204166	1.0282275250546027

(b) Snapshot of the file containing some relevant parameters of ESO 533-004: 'results_ESO533-004.csv'.

Figure 11: Image showing the two files with the results of ESO 533-004.

In the big picture, steps 2 through 8 all happen inside the `scipy.optimize.curve_fit` routine. This routine keeps changing the values of $(\rho_{\rm T}|_{z=0})/(\rho_{\rm t}|_{z=0})$, $\sigma_{\rm T}/\sigma_{\rm t}$ and f repeating steps 2 through 8 until the algorithm converges. Fig. 10 shows a simplified flow diagram that explains the whole process.

2.6 Outputs of the fit

The final step of the code is to save the results. For this, a number of files are created: for each bin an archive named `galaxyname_bin_number` saves the columns shown in Fig. 11a: the z axis in arcseconds `Height_z_in_arcsec`, the observed surface brightness profile in magnitudes `Observed_profile_in_mag`, the best fit to the observed profile `Fit_profile_in_mag`, and the best models to the contributions of the thin and thick discs, `Fit_of_thin_disc_in_mag` and `Fit_of_thick_disc_in_mag`, respectively.

Additionally, another file named `results_galaxyname.csv` contains all the relevant parameters of the fits for each galaxy, as shown in Fig. 11b. The bin number, its position and width, the fitted three free parameters of the fit $(\rho_{\rm T}|_{z=0})/(\rho_{\rm t}|_{z=0})$, $\sigma_{\rm T}/\sigma_{\rm t}$ and f, the ratio of the mass-to-light ratios of the thick and thin discs at 3.6μm $(\Upsilon_{\rm T}/\Upsilon_{\rm t})_{3.6\mu{\rm m}}$, the final dynamic range $\Delta\mu$, the RMSE value of the fit, and the thick to thin disc surface density ratio $\Sigma_{\rm T}/\Sigma_{\rm t}$.

3 Results and Discussion

To verify the reliability of our recently developed code we need to compare our results with the previously obtained ones by Comerón et al. (2018) using the original IDL code. For that, we have extracted the surface brightness profiles of the galaxies ESO 533-004 and NGC 4565. As mentioned in Section 2.2.2, the selected bins are centred at positions $(-0.65, -0.35, 0.35, 0.65) \times R_{\rm opt}$ with a $0.30 \times R_{\rm opt}$ width.

Tables 1 and 2 contain the most relevant parameters of ESO 533-004 and NGC 4565, respectively, obtained from the fits. Subtables

1a and 2a show the bin numbers and the free parameters of the fit for each one, along with the RMSE value of the fit, while subtables 1c and 2c include other parameters, mentioned in Section 2.6. In the following paragraphs we will be commenting on some of these parameters.

3.1 Discussion for ESO 533-004

The first parameter of the fit $(\rho_{\rm T}|_{z=0})/(\rho_{\rm t}|_{z=0})$ compares the density of a thick disc component to that of a thin disc component at the mid-plane of the galaxy ($z = 0$). These ratios provide information on the relative contributions of the thick and thin disc components to the overall structure of the galaxy. All values are < 1, which translates into the dominance of the thin disc over the thick disc near the mid-plane. Except for the first bin, our values are remarkably close to those of (Comerón et al., 2018), with a maximum deviation of 9.5%.

The next parameter is the ratio of velocity dispersions $\sigma_{\rm T}/\sigma_{\rm t}$. This ratio compares the velocity dispersion of the thick disc to that of the thin disc of a galaxy. In our results these ratios are consistently above 2, indicating a significant difference in velocity dispersion between the thick disc and the thin disc. Such high ratios suggest that the thick disc has a much higher velocity dispersion compared to the thin disc across these bins. This implies that the thick disc and thin disc are distinct components within the galaxy and could suggest different formation mechanisms or evolutionary histories for these two components. If $\sigma_{\rm T}/\sigma_{\rm t}$ were close to 1, the velocity dispersions of both discs would be very similar and the distinction between them would blur, thus preventing to be identified as two different discs. Comparing with the values of Comerón et al. (2018), their ratios are around 1.9, indicating a smaller difference in velocity dispersion between the thick and thin discs.

The last parameters in Subtable 1a are the surface brightness values $\mu_{\rm c}$ where the fit and the observed profile meet, also defined as the central surface brightness multiplied by the aforementioned factor f and then converted to magnitudes, and the RMSE of the fit. The values of the latter are all under $0.1\,{\rm mag\,arcsec^{-2}}$, authenticating the reliability of the fit.

The third subtable displays in the first three columns the information about the selected bins mentioned in Section 2.2.2. The most relevant information in this subtable is the surface density ratios $\Sigma_{\rm T}/\Sigma_{\rm t}$, that indicate the relationship between the surface densities of the thick disc and the thin disc for each respective bin in the galaxy. The surface densities were calculated from the integration of the density profiles along the z axis. For bins 1 and 2 $\Sigma_{\rm T}/\Sigma_{\rm t} < 1$, and this suggests that the surface density of the thick disc is significantly lower than that of the thin disc in these regions, while for bins 3 and 4 the opposite happens. In Comerón et al. (2018) we see that all the ratios are $\Sigma_{\rm T}/\Sigma_{\rm t} < 1$ for ESO 533-004. Except for bin 1, our $\Sigma_{\rm T}/\Sigma_{\rm t}$ values are not too different given differences of the order of 20%.

Fig. 12 shows the surface brightness profiles obtained for ESO 533-004 in the bins mentioned in Section 2.2.2. The top figure are the results from our new code, while the one on the bottom depicts the results of Comerón et al. (2018). Each panel corresponds to a bin and has some of the relevant parameters of Table 1. Bins 2 and 3 both have a higher

Bin number	$(\rho_T\|_{z=0})/(\rho_t\|_{z=0})$	σ_T/σ_t	μ_c (mag arcsec^{-2})	RMSE (mag arcsec^{-2})
1	0.18	2.14	22.63	0.05
2	0.21	2.14	22.28	0.04
3	0.35	2.50	21.36	0.09
4	0.34	2.34	22.00	0.08

(a) Free parameters of the fit and the RMSE value of each bin.

Bin number	$(\rho_T\|_{z=0})/(\rho_t\|_{z=0})$	σ_T/σ_t	RMSE (mag arcsec^{-2})
1	0.40	1.84	0.087
2	0.23	1.89	0.088
3	0.35	1.93	0.070
4	0.36	1.99	0.086

(b) Free parameters of the fit and the RMSE value of each bin in Comerón et al. (2018)'s results.

Bin number	Bin's central position (R_{opt})	Bin's width (R_{opt})	z_c (arcsec)	$\Delta\mu$ (mag arcsec^{-2})	$\frac{\Sigma_T}{\Sigma_t}$	$\left(\frac{\Upsilon_T}{\Upsilon_t}\right)_{3.6\mu m}$
1	−0.65	0.30	6.82	5.0	0.49	1.2
2	−0.35	0.30	7.33	6.0	0.58	1.2
3	0.35	0.30	4.86	7.0	1.15	1.2
4	0.65	0.30	5.04	6.0	1.03	1.2

(c) Other parameters of the fit.

Bin number	Bin's central position (R_{opt})	Bin's width (R_{opt})	$\Delta\mu$ (mag arcsec^{-2})	$\frac{\Sigma_T}{\Sigma_t}$	$\left(\frac{\Upsilon_T}{\Upsilon_t}\right)_{3.6\mu m}$
1	−0.65	0.30	5.5	0.93	1.2
2	−0.35	0.30	7.0	0.56	1.2
3	0.35	0.30	6.0	0.87	1.2
4	0.65	0.30	5.5	0.93	1.2

(d) Other parameters of the fit of Comerón et al. (2018).

Table 1: Table showing the outputs of the code named in Section 2.6 for ESO 533-004.

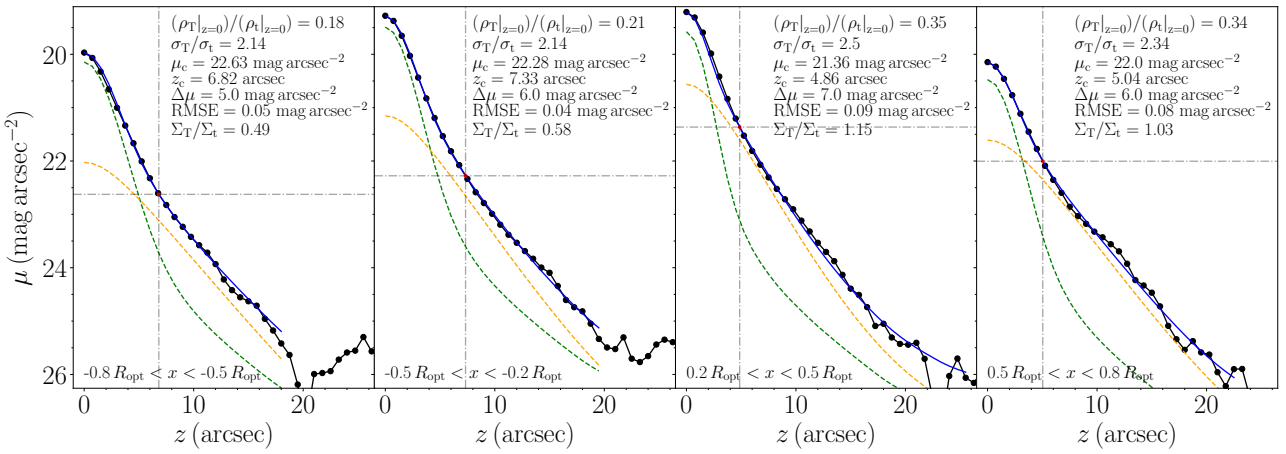

(a) Our results for ESO 533-004. The black dots are the extracted observed data points. The blue line represents the model of the total surface brightness profile. The green and yellow dashed lines are the models of the thin and thick discs, respectively.

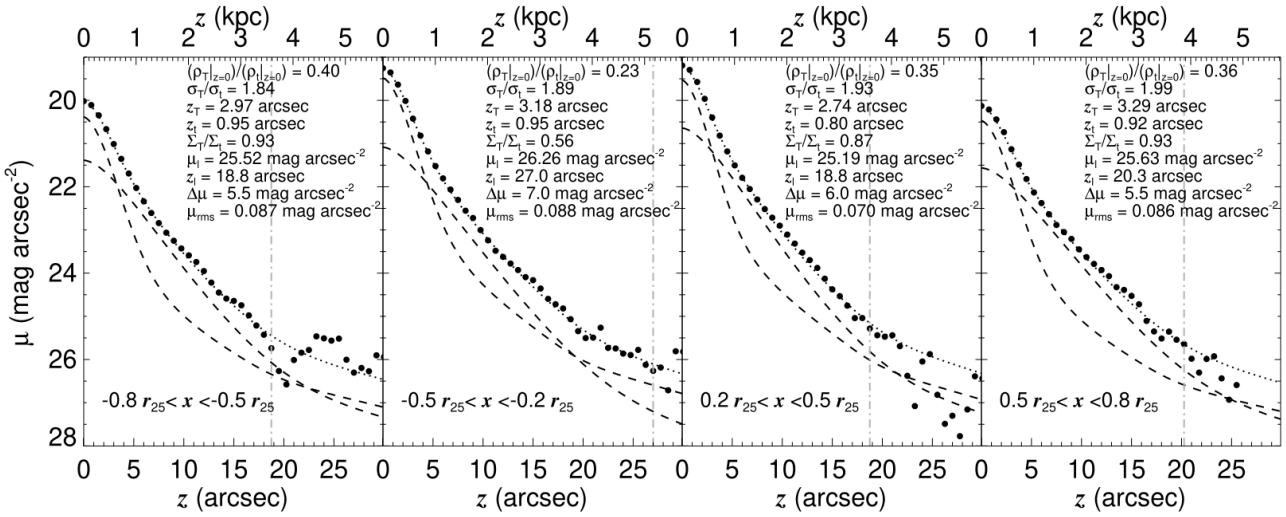

(b) Results for ESO 533-004 of Comerón et al. (2018). The bigger black dots are the data points of the observed surface brightness profile. The dotted line is the model of the total surface brightness profile. The dashed lines are the thin and thick disc components.

Figure 12: Results for ESO 533-004.

surface brightness in the mid-plane than bins 1 and 4, since they are nearer to the galactic centre. The blue model overall follows the trend of the observed profile quite well across all panels. This indicates that the model accurately represents the surface brightness distribution in these regions of the galaxy.

The thin disc model fits the data well at low height values, being the dominant component at the mid-plane neighbourhood. As z increases, the thin disc model is not sufficient to explain the observed data, indicating a less significant contribution to the surface brightness at higher z values where the thick disc begins to dominate. For bins 2 and 3 the thin disc seems to start dominating again for large z values. This is due to the LSF convolution and illustrates the importance of taking this effect into account.

3.2 Discussion for NGC 4565

Bin number	$(\rho_T\|_{z=0})/(\rho_t\|_{z=0})$	σ_T/σ_t	μ_c (mag arcsec^{-2})	RMSE (mag arcsec^{-2})
1	0.29	2.12	23.97	0.10
2	0.03	2.75	22.53	0.08
3	0.05	2.46	22.11	0.08
4	0.05	3.52	23.44	0.08

(a) Free parameters of the fit and the RMSE value of each bin.

Bin number	$(\rho_T\|_{z=0})/(\rho_t\|_{z=0})$	σ_T/σ_t	RMSE (mag arcsec^{-2})
1	0.57	2.07	0.045
2	0.03	2.49	0.069
3	0.03	2.57	0.069
4	0.04	3.14	0.079

(b) Free parameters of the fit and the RMSE value of each bin in Comerón et al. (2018)'s results.

Bin number	Bin's central position (R_{opt})	Bin's width (R_{opt})	z_c (arcsec)	$\Delta\mu$ (mag arcsec^{-2})	$\frac{\Sigma_T}{\Sigma_t}$	$\left(\frac{\Upsilon_T}{\Upsilon_t}\right)_{3.6\mu m}$
1	−0.65	0.30	30.99	4.5	0.77	1.2
2	−0.35	0.30	29.49	6.5	0.12	1.2
3	0.35	0.30	25.84	5.5	0.18	1.2
4	0.65	0.30	25.99	5.0	0.29	1.2

(c) Other parameters of the fit.

Bin number	Bin's central position (R_{opt})	Bin's width (R_{opt})	$\Delta\mu$ (mag arcsec^{-2})	$\frac{\Sigma_T}{\Sigma_t}$	$\left(\frac{\Upsilon_T}{\Upsilon_t}\right)_{3.6\mu m}$
1	−0.65	0.30	4.5	1.46	1.2
2	−0.35	0.30	7.0	0.12	1.2
3	0.35	0.30	6.5	0.14	1.2
4	0.65	0.30	5.5	0.23	1.2

(d) Other parameters of the fit in Comerón et al. (2018)'s results.

Table 2: Table showing the outputs of the code named in Section 2.6 for NGC 4565.

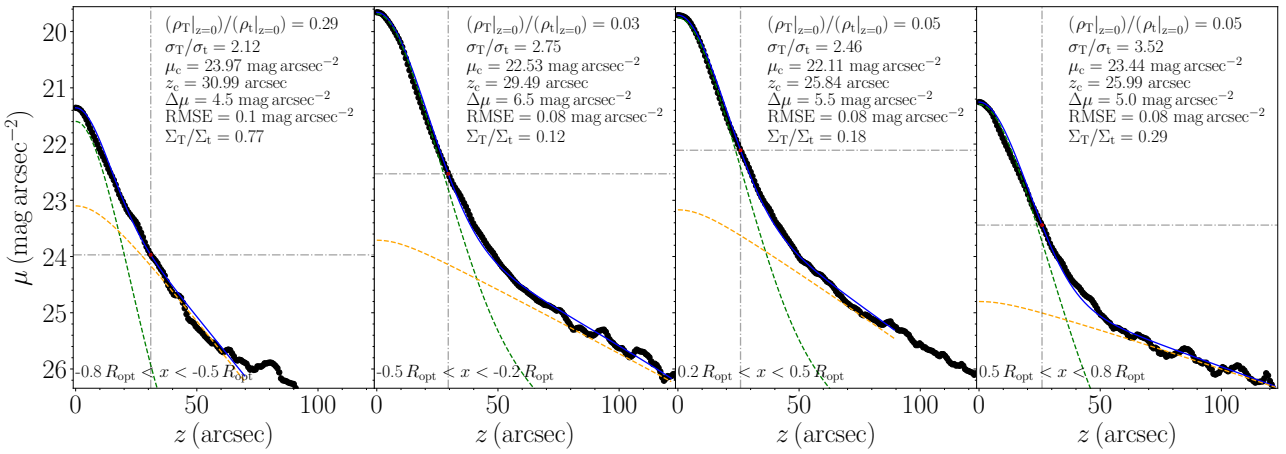

(a) Our results for NGC 4565. The black dots are the extracted observed data points. The blue line represents the model of the total surface brightness profile. The green and yellow dashed lines are the models of the thin and thick discs, respectively.

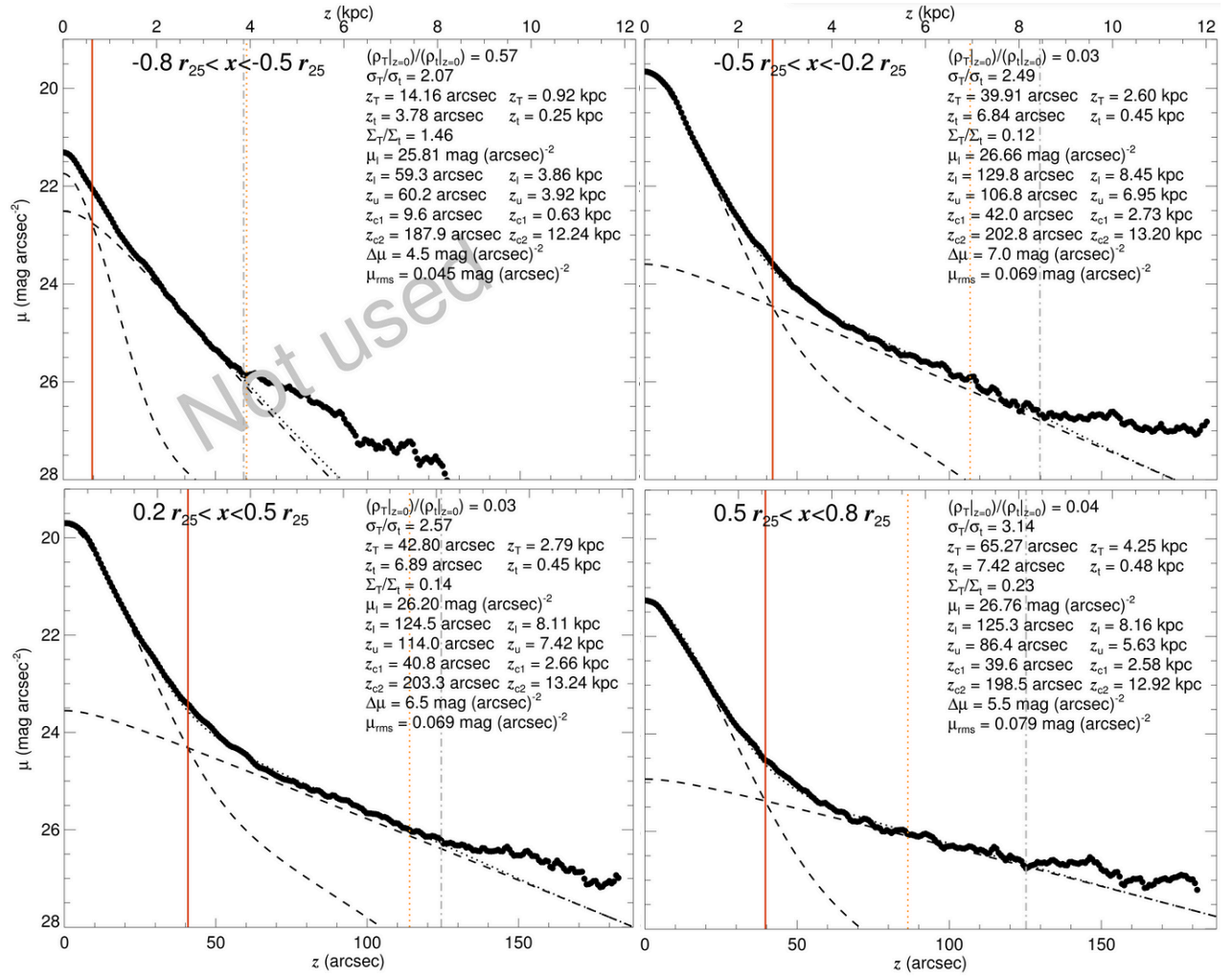

(b) Results for NGC 4565 of Comerón et al. (2018). The larger black dots are the data points of the observed surface brightness profile. The dotted line is the model of the total surface brightness profile. The dashed lines are the thin and thick disc components.

Figure 13: Results for NGC 4565.

Just like for ESO 533-004, Table 2 shows the outputs of the code. The first thing we notice is that the values of $(\rho_{\rm T}|_{z=0})/(\rho_{\rm t}|_{z=0})$ are much smaller than for ESO 533-004. This means that NGC 4565 has a much smaller contribution of the thick disc in the mid-plane. Again, save for the first bin, our results are very similar to the ones of Comerón et al. (2018).

The ratios of velocity dispersions $\sigma_{\rm T}/\sigma_{\rm t}$ of NGC 4565 closely match those of ESO 533-004. Our results present a similarity in the relation of velocity dispersions of NGC 4565 and ESO 533-004. Again, the fact that all ratios are > 1 states that the thin disc has a much lower velocity dispersion compared to the thick disc, translating into a clear distinction of both components. The results of Comerón et al. (2018) reflect similar values to ours'. However, in their case, these ratios are larger than the ones for ESO 533-004. According to their results, the difference between the velocity dispersions of the thick and thin discs is much larger for NGC 4565 than for ESO 533-04.

The last parameter in Table 2a attests to the reliability of the fits. For bin 1 the RMSE value is RMSE $= 0.1\,\mathrm{mag\,arcsec^{-2}}$, the maximum value of RMSE we defined for a model to be a good fit. As a consequence, the fit did not go down to a larger dynamic range of $\Delta\mu = 5\,\mathrm{mag\,arcsec^{-2}}$.

For $\Sigma_{\rm T}/\Sigma_{\rm t}$ in Subtable 2c we see that all values are smaller than 1, indicating that the thin disc has a higher surface density value in these regions of the galaxy. Both in our results and in Comerón et al. (2018)'s results the volume density at the mid-plane and the surface density of the thick disc are larger in bin nº1, this is, in the $-0.8\,R_{\rm opt} < x < -0.5\,R_{\rm opt}$ region. Not only that, but the surface density ratio of Comerón et al. (2018) for this region is $\Sigma_{\rm T}/\Sigma_{\rm t} > 1$. The problems with this bin are natural, as its RMSE indicates that the fit is not good enough. A possible reason is that for this bin $\mu|_{z=0} + \Delta\mu = 25.8\,\mathrm{mag\,arcsec^{-2}}$, which is very close to the limiting magnitude of the S^{4}G $\mu_{3.6\mu\mathrm{m}} = 26.5(\mathrm{AB})\,\mathrm{mag\,arcsec^{-2}}$. Perhaps the image is not deep enough to obtain a proper fit, or the galaxy is perturbed in its outskirts and the assumption of hydrostatic equilibrium does not hold in those regions.

Fig 13 shows the calculated results for NGC 4565, both ours' and the ones of Comerón et al. (2018). The blue line follows quite accurately the observed surface brightness profile, with RMSE values lower than $0.1\,\mathrm{mag\,arcsec^{-2}}$. As seen for ESO 533-004 the thin disc dominates the mid-plane region, while the thick disc starts to gain protagonism at large heights.

3.3 Discrepancy in results

In the section above we discussed some differences between the results of Comerón et al. (2018) and ours'. This is a consequence of different approaches on some parts of the code.

The gas in a galaxy, mostly composed of atomic Hydrogen H I and molecular Hydrogen H II, lies within a disc often referred to as the 'gas disc' in the plane of the galaxy. Unlike us, Comerón et al. (2018) account for the gas disc in their equations for the creation of the model:

$$\frac{d^2\rho_{\rm i}}{dz^2} = \frac{\rho_{\rm i}}{\sigma_{\rm i}^2}\left[-4\pi G\left(\rho_{\rm t} + \rho_{\rm T} + \rho_{\rm g}\right)\right] + \frac{1}{\rho_{\rm t}}\left(\frac{d\rho_{\rm t}}{dz}\right)^2, \tag{6}$$

where t, T, and g denote the thin, the thick, and the gas disc, respectively. By not taking the gas disc into account it is reasonable to have different results, since the effect of having a gas disc is to slightly shrink the scale-height of the thin disc for a given $\sigma_{\rm t}$.

In the selection of bins in Sect. 2.2.2 the central area is avoided. This is because in that region the galactic bulge dominates. However, the bulge can still affect the bins that we have studied, especially when smeared by the PSF, so modelling the effect of the bulge in the selected bins could probably improve our results, as done in Comerón et al. (2018) where the bulge was modelled and its contribution was removed from the surface brightness profiles before doing the fits.

As explained in Sect. 2.1.2, we used a Line Spread Function, obtained from the convolution of an infinitesimally thin distribution of light with an infinite extension with the PSF of the warm mission model of the S^{4}G at 3.6μm. Comerón et al. (2018) made use of an infinitesimally thin distribution of light with an exponential scale-length, which is a more realistic representation of how light is distributed in a galactic disc.

Another factor that could alter our results is that we interpolate over the masked pixels of the 2D image instead of ignoring them like Comerón et al. (2018) did. The presence of some missing data might not significantly impact the results, but we believe that for the study of the vertical structure of edge-on galaxies interpolation can be beneficial as it ensures data continuity and facilitates the fitting of the model.

Lastly, an aforementioned detail is that we implement the factor f as a free parameter in the fitting process, whereas Comerón et al. (2018) have a set of constant values to choose from. Introducing this factor as a free parameter leads to a more accurate model of the observed surface brightness profile.

3.4 Downsizing

The downsizing theory in galaxy formation posits that the most massive galaxies evolved faster than the lowest mass ones (Cowie et al., 1996). This implies that for the massive galaxies the bulk of their stars formed early in the history of the Universe, completing their star formation processes quickly. In contrast, smaller galaxies form stars more gradually, continuing their star formation over longer periods of time.

In the discussion of the Σ_T/Σ_t parameter we realised that for NGC 4565 these ratios are much smaller than for ESO 533-004. This could mean that NGC 4565 has a more developed thin disc. If we apply the concept of downsizing to the thin and thick disc formation this could imply that thick discs form first and thin discs in low-mass galaxies are not fully developed (Comerón, 2021). This agrees with the fact that NGC 4565 is a more massive galaxy than ESO 533-004. To confirm this, we can get the total masses of these galaxies by adding the masses of each component provided by Comerón et al. (2018), estimating a mass of $34.14 \times 10^9\,\mathcal{M}_\odot$ for ESO 533-004 and a mass of $139.79 \times 10^9\,\mathcal{M}_\odot$ for NGC 4565.

These deductions have been made with the information obtained from only two galaxies, ESO 533-004 and NGC 4565. However, these conclusions seem to be general, as shown in Fig. 2.

3.5 Future implementations

For the possible future continuation of the project, we suggest the following implementations to enhance the accuracy and consistency of our model:

1. Incorporation of the gas disc, by assigning to gas a fraction of the stellar mass of the

galaxy based on models or estimating it from H I data if available.

2. Modelling the effect of the galactic bulge.
3. Using an exponential scale-length for the obtention of the LSF.
4. Introduction of case-by-case Υ_T/Υ_t values by studying colours at different heights z and deducing the individual mass-to-light ratios Υ_T and Υ_t.

We aim to apply this code to galaxies at different redshifts observed using *HST* and *JWST* to see whether the thick or thin disc forms first, in order to probe formation mechanisms. Observations at high redshift capture galaxies in their formation stages, providing a glimpse into the emergence of thin and thick discs and the processes that may contribute to their evolution.

4 Summary and conclusions

In a nutshell, this newly developed code generates surface brightness profiles in different regions of an edge-on galaxy and fits them to a synthetic profile created using thin and thick disc models obtained by numerically solving the hydrostatic equilibrium equations for two coupled isothermal discs.

The methodology employed in this study integrates advanced observational techniques with sophisticated modelling approaches to dissect the structural evolution of disc galaxies. The choice of galaxies, ESO 533-004 and NGC 4565, both galaxies from the S^{4}G taken at 3.6 μm, was strategic, leveraging their clarity and suitability for detailed comparative analysis with the results of Comerón et al. (2018).

A significant challenge addressed in this study was taking into account scattered light effects, which can distort the observed light distribution of galaxies, in the synthetic profiles. Addressing this, the Line Spread Function (LSF) was used to model the effects of the optical imaging system on the synthetic profiles.

The preprocessing of the observational data involved rigorous steps to enhance data quality and precision. These included subtracting the sky background and interpolating over masked regions to fill gaps in data. To optimize the analysis of surface brightness profiles, axial bins were strategically selected to capture variations across the radius of the galaxy.

To derive surface brightness profiles an iterative process was employed, involving shifting the images to determine the mid-plane of the galaxy with a subpixel precision. Synthetic profiles were generated through the resolution of the differential equations of two coupled isothermal discs in hydrostatic equilibrium, simulating the vertical density profiles of the discs in the galaxies, later transformed into surface brightness profiles. These models were carefully scaled and fitted to the observed data.

After solving differential equations to model surface brightness profiles, the next crucial step is convolution. This process integrates the model surface brightness profile with the Line Spread Function (LSF), essential for comparing it with observed data. In this study, the `scipy.signal.convolve()` routine of Python was employed.

Achieving a precise fit of the contributions of the thin and thick discs needs an iterative approach. This process starts with a minimum dynamic range $\Delta\mu = 4.5\,\mathrm{mag\,arcsec^{-2}}$. Iteratively increasing by $0.5\,\mathrm{mag\,arcsec^{-2}}$, the Root Mean Square Error

(RMSE) is monitored to ensure convergence with a RMSE below $0.1\,\mathrm{mag\,arcsec^{-2}}$, indicating a reliable fit.

In the process of verification of the model reliability against previous studies (Comerón et al., 2018) we conclude that:

- The fitted parameters $(\rho_\mathrm{T}|_{z=0})/(\rho_\mathrm{t}|_{z=0})$ and $\sigma_\mathrm{T}/\sigma_\mathrm{t}$ demonstrate consistency, with minor deviations from those of Comerón et al. (2018), confirming model robustness.
- The ratio of thick to thin disc surface densities $\Sigma_\mathrm{T}/\Sigma_\mathrm{t}$ indicates a relative smaller contribution of the thick disc in NGC 4565 compared to ESO 533-004, suggesting a more prominent thin disc in the former. This observation aligns with the downsizing theory and the hypothesis that thick discs form first, which posits that more massive galaxies, like NGC 4565, are more evolved and have more developed thin discs.
- The obtained ratios $\sigma_\mathrm{T}/\sigma_\mathrm{t}$ indicate a significant difference in velocity dispersion between the thin and thick disc, suggesting distinct evolutionary paths or formation mechanisms for the thick and thin discs.
- Discrepancies between our and Comerón et al. (2018)'s results probably stem from methodological variances. Factors such as the exclusion of the gas disc in our model, the handling of masked pixels through interpolation, the use of a simplified LSF model and the incorporation of the factor f as a free parameter influence model accuracy.
- Future implementations could include incorporating the gas disc, modelling the galactic bulge effect, refining the LSF model, and potentially introducing a variable $\Upsilon_\mathrm{T}/\Upsilon_\mathrm{t}$ to enhance the model accuracy.

References

Abadi M. G., Navarro J. F., Steinmetz M., Eke V. R., 2003a, ApJ, 591, 499

Abadi M. G., Navarro J. F., Steinmetz M., Eke V. R., 2003b, ApJ, 597, 21

Bensby T., Feltzing S., Lundström I., Ilyin I., 2005, A&A, 433, 185

Bournaud F., Elmegreen B. G., Martig M., 2009, ApJ, 707, L1

Brook C. B., Kawata D., Gibson B. K., Freeman K. C., 2004, ApJ, 612, 894

Burstein D., 1979, ApJ, 234, 829

Comerón S., 2021, A&A, 645, L13

Comerón S., et al., 2011a, ApJ, 738, L17

Comerón S., et al., 2011b, ApJ, 741, 28

Comerón S., et al., 2012, ApJ, 759, 98

Comerón S., Elmegreen B. G., Salo H., Laurikainen E., Holwerda B. W., Knapen J. H., 2014, A&A, 571, A58

Comerón S., Salo H., Janz J., Laurikainen E., Yoachim P., 2015, A&A, 584, A34

Comerón S., Salo H., Peletier R. F., Mentz J., 2016, A&A, 593, L6

Comerón S., Salo H., Knapen J. H., 2018, A&A, 610, A5

Comerón S., Salo H., Knapen J. H., Peletier R. F., 2019, A&A, 623, A89

Cowie L. L., Songaila A., Hu E. M., Cohen J. G., 1996, AJ, 112, 839

De Jong R. S., 2008, MNRAS, 388, 1521

Elmegreen B. G., Elmegreen D. M., 2006, ApJ, 650, 644

Elmegreen B. G., Elmegreen D. M., Tompkins B., Jenks L. G., 2017, ApJ, 847, 14

Gilmore G., Reid N., 1983, MNRAS, 202, 1025

Hora J. L., et al., 2012, in Clampin M. C., Fazio G. G., MacEwen H. A., Oschmann Jacobus M. J., eds, Society of Photo-Optical Instrumentation Engineers (SPIE) Conference Series Vol. 8442, Space Telescopes and Instrumentation 2012: Optical, Infrared, and Millimeter Wave. p. 844239, doi:10.1117/12.926894

Kormendy J., Kennicutt Robert C. J., 2004, ARA&A, 42, 603

Martig M., Minchev I., Flynn C., 2014a, MNRAS, 442, 2474

Martig M., Minchev I., Flynn C., 2014b, MNRAS, 443, 2452

Muñoz-Mateos J. C., et al., 2015, ApJS, 219, 3

Narayan C. A., Jog C. J., 2002, A&A, 394, 89

Nykytyuk T. V., Mishenina T. V., 2006, A&A, 456, 969

Pinna F., et al., 2019a, A&A, 623, A19

Pinna F., et al., 2019b, A&A, 625, A95
Prochaska J. X., Naumov S. O., Carney B. W., McWilliam A., Wolfe A. M., 2000, AJ, 120, 2513
Qu Y., Di Matteo P., Lehnert M. D., van Driel W., 2011a, A&A, 530, A10
Qu Y., Di Matteo P., Lehnert M. D., van Driel W., Jog C. J., 2011b, A&A, 535, A5
Roškar R., Debattista V. P., Loebman S. R., 2013, MNRAS, 433, 976
Sandin C., 2015, A&A, 577, A106
Schönrich R., Binney J., 2009a, MNRAS, 396, 203
Schönrich R., Binney J., 2009b, MNRAS, 399, 1145
Sheth K., et al., 2010, PASP, 122, 1397
Tsikoudi V., 1979, ApJ, 234, 842
Villumsen J. V., 1983, ApJ, 274, 632

Appendix: individual surface brightness profiles of each bin for galaxies ESO 533-004 and NGC 4565.

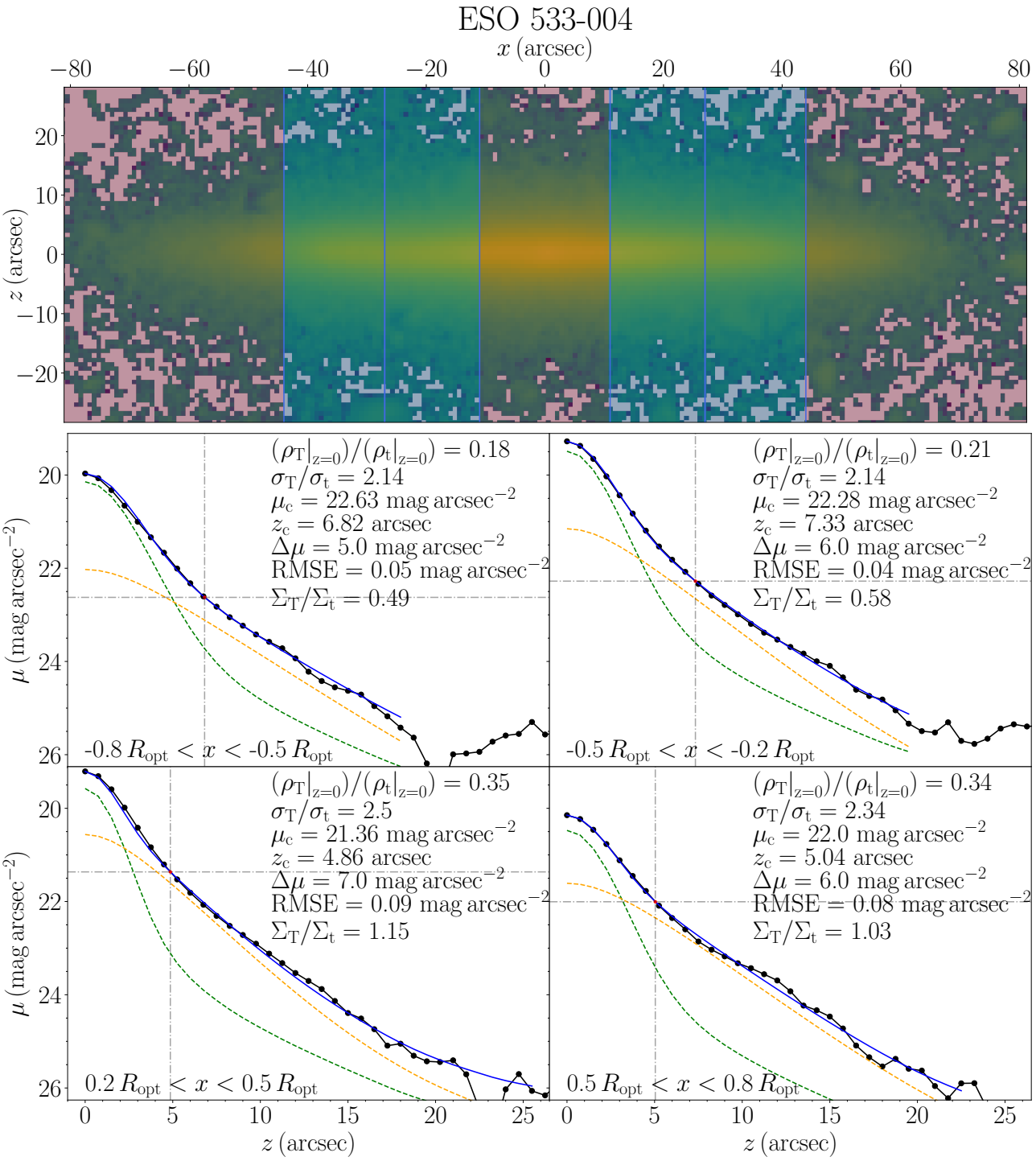

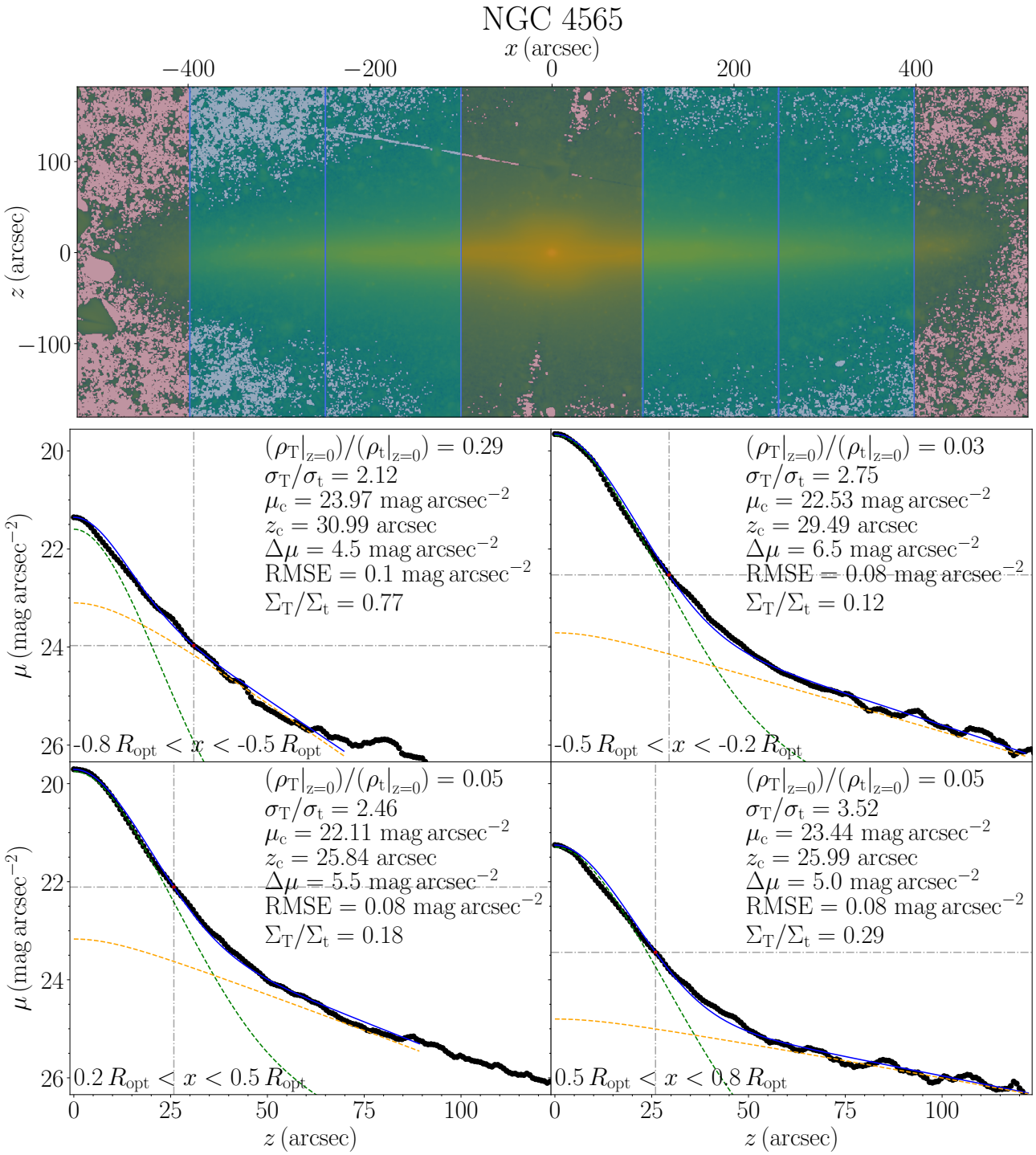
NGC 4565
x (arcsec)
−400
−200
0
200
400
100
0
−100
z (arcsec)
(ρT|z=0)/(ρt|z=0) = 0.29
σT/σt = 2.12
μc = 23.97 mag arcsec−2
zc = 30.99 arcsec
Δμ = 4.5 mag arcsec−2
RMSE = 0.1 mag arcsec−2
ΣT/Σt = 0.77
-0.8 Ropt < x < -0.5 Ropt
(ρT|z=0)/(ρt|z=0) = 0.03
σT/σt = 2.75
μc = 22.53 mag arcsec−2
zc = 29.49 arcsec
Δμ = 6.5 mag arcsec−2
RMSE = 0.08 mag arcsec−2
ΣT/Σt = 0.12
-0.5 Ropt < x < -0.2 Ropt
(ρT|z=0)/(ρt|z=0) = 0.05
σT/σt = 2.46
μc = 22.11 mag arcsec−2
zc = 25.84 arcsec
Δμ = 5.5 mag arcsec−2
RMSE = 0.08 mag arcsec−2
ΣT/Σt = 0.18
0.2 Ropt < x < 0.5 Ropt
(ρT|z=0)/(ρt|z=0) = 0.05
σT/σt = 3.52
μc = 23.44 mag arcsec−2
zc = 25.99 arcsec
Δμ = 5.0 mag arcsec−2
RMSE = 0.08 mag arcsec−2
ΣT/Σt = 0.29
0.5 Ropt < x < 0.8 Ropt
μ (mag arcsec−2)
20
22
24
26
0
25
50
75
100
z (arcsec)